UNITED NATIONS UNIVERSITY
UNU-GTP
Geothermal Training Programme

Orkustofnun, Grensasvegur 9,
IS-108 Reykjavik, Iceland

Reports 2015
Number 23

MICROGRAVITY SURVEY IN 2009-2010 AROUND BACMAN GEOTHERMAL FIELD, PHILIPPINES - GRAVITY CORRECTIONS AND INTERPRETATIONS

Jonathan Lee C. Monasterial
Energy Development Corporation - EDC
38/F One Corporate Centre Building
Julia Vargas corner Meralco Avenue
OrtigasCenter, Pasig City, 1605
PHILIPPINES
monasterial.jc@energy.com.ph

ABSTRACT

A microgravity survey was conducted in 2009-2010 around the Bacman geothermal field, Philippines. The observed gravity readings were subjected to the standard reduction process such as tidal, instrumental drift, latitude, and terrain corrections using Gravos, Gnet, Terra and Terrb reduction programs. Free-air and Bouguer corrections were calculated by using the Bouguer program. After these corrections, the optimum reduction density was determined analytically by using the Parasnis method. To enhance the local anomalies, the regional trend in the Bouguer maps was removed. The regional field was estimated to be planar.

Positive anomalies in the central part of the field are within the Bacman Fault Zone. These are interpreted to be dense, intrusive rocks such as diorite which are present beneath this area based on core samples. In addition, these anomalies extend to the western and northern regions of the field near Mts. Tikolob and Kayabon and may be related to the resistivity anomaly seen in the western part of the field. Negative anomalies represent the sedimentary formations and collapse features in the south-eastern and northern parts of the area, respectively.

Using limiting depth analysis, the dense intrusive rock was approximated as a spherical body and its centre was found to be at a depth of around 900 m. In addition, an irregularly shaped body was assumed to be present beneath the western parts of the field and a depth to the top of this body was found to be about 1750 m.

1. INTRODUCTION

Geothermal energy has become increasingly important around the world for the past few decades. This renewable energy has been utilized for electricity generation in 24 countries. In total globally, around 12.35 GWe of installed capacity are projected for this year, which is an increase of 16% compared to 2010. USA, Philippines, Indonesia, Mexico and New Zealand are among the leading countries in terms of installed electrical power capacity (Bertani, 2015). Moreover, this clean energy is also used directly

in 82 countries worldwide for ground-source heat pumps, bathing and swimming pools, space heating, greenhouses, etc. Globally, the total installed thermal power is around 70.329 GWth, an increase by 45% compared with the data gathered in 2010 (Lund and Boyd, 2015). Countries with the largest installed capacities include China, USA, Sweden, Turkey and Iceland. In terms of primary energy supply available, geothermal energy is very small compared to other sources such as oil, coal, and natural gas which comprise 31.4%, 29.0%, and 21.3%, respectively, of the total primary energy supply worldwide (IEA, 2014). More geothermal energy development is needed in order to increase the supply coming from this green and clean energy. However, geothermal energy development, like any other energy development, needs to start with scientific investigation and exploration. Effective methods of exploration are crucial for the successful development of geothermal resources due to the complexity of subsurface geothermal systems. In general, geothermal exploration should be done with a multidisciplinary approach which focuses on geology, geochemistry and geophysics. Geological exploration methods include mapping of tectonic structures, stratigraphy and hydrothermal alteration, as well as geological history. Geochemical studies on surface manifestations such as hot springs and fumaroles are done to evaluate fluid properties and estimate reservoir temperature. Geophysical surveys are used to detect and image subsurface structures related to geothermal systems and estimate the reservoir size and properties and together with other observations to locate possible drilling targets (Flóvenz et al., 2012).

Most geophysical methods are passive, i.e. they are based on natural changes. These include magnetotelluric (MT), seismic, magnetic, and gravity methods. The seismic methods use natural seismicity to obtain information that may be related to fluid movement within geothermal systems, as well as information on velocity structures. In the magnetic method, which is a potential method, spatial variations in the earth's magnetic field strength are measured. Magnetic maps are then generated which represent the variations of magnetic properties of subsurface features. The gravity method, which is also a potential method, is used in a similar way. These methods are used to identify structures such as faults, dykes and intrusions by measuring spatial variations in gravitational acceleration and magnetic intensity due to lateral changes of density and susceptibility of the earth. The field variations can, in many cases, be interpreted by using analytical modelling and thereby give an idea about the depth, geometry and density or susceptibility causing them (Mariita, 2007). On the other hand, active methods do not rely on natural changes but use artificial signal sources, such as in seismic refraction and reflection and transverse electromagnetic (TEM) methods.

The gravity method is the main objective of this report. This report focuses particularly on the microgravity survey conducted at the Bacman geothermal field (BGF) in the provinces of Albay and Sorsogon of the Philippines in 2009 and 2010. Previous and most recent geophysical surveys in the area are briefly presented. Microgravity data processing, analysis and interpretation are discussed in detail in this report.

2. GRAVITY CONCEPTS AND PRINCIPLES

Newton's law of gravitation states that the attractive force F between two bodies is directly proportional to the product of the masses and inversely proportional to the square of the distance between the centres of mass of the bodies. It is given by:

$$F = G\frac{m_1 m_2}{r^2} \tag{1}$$

where G = Universal gravitational constant [Nm^2/kg^2] in SI units;
m_1 = Mass of the first body [kg];
m_2 = Mass of the second body [kg];
r = Distance between the centres of masses of the particles [m].

Based on Newton's Second Law of Motion, which states that force is the product of mass and acceleration, Equation 1 can be rearranged into:

$$F = m_1 G \frac{m_2}{r^2} = m_1 g_2 \quad (2)$$

where g_2 = Acceleration due to gravitational force of the second body of mass m_2 on unit mass of the first body [m/s^2].

In Equation 2, if m_1 is free to move, it will be drawn towards m_2 at a speed which constantly increases with acceleration g_2 (Hunt, 2001). For the case of Earth, g_2 becomes the acceleration of gravity g_e on the surface of the earth and is given by:

$$g_e = G \frac{M_e}{{R_e}^2} \quad (3)$$

where R_e = Radius of the Earth [m];
M_e = Mass of the Earth [kg].

The force of gravity is a derivative of a potential field which has no gaps or discontinuities. The gravitational force at a point can be presented by a vector whose magnitude and direction is the sum of the attraction of all bodies in the universe. In general, the force of gravity at any point on the Earth's surface is mainly due to the Earth itself with minor contributions from the sun and moon (Hunt, 2001).

The acceleration of gravity due to Earth was first measured by Galileo Galilei in his famous experiment at Pisa. Two equivalent SI units can be used for acceleration which is metres per second squared (m/s^2) and Newton per kilogram (N/kg). The value for the acceleration of the earth is 9.8 m/s^2 on the average but varies with latitude and elevation. In geophysics, the most commonly used unit of gravity is Gal, named after Galileo, 1 Gal = 1cm/s^2 = 10^{-2} m/s^2. In gravity measurements, 1 milligal (mgal) = 10^{-5} m/s^2 and 1 microgal (μgal) = 10^{-8} gal. Furthermore, a commonly used unit is gravity unit (gu) which is equivalent to 0.1 mgal.

The Earth´s gravitational potential is defined as:

$$U = G \frac{M_e}{r} \quad (4)$$

where U = Gravitational potential [J/kg];
r = Distance from the centre of mass of Earth [m].

In Equation 4, the gravitational potential field U is a scalar quantity and its first derivative in any direction gives the acceleration of gravity in that direction. Equipotential surfaces on earth are surfaces where U is constant. The sea-level surface, or the geoid, is the most easily recognized equipotential surface. It is horizontal, that is at a right angle to the gravitational acceleration (Kearey et al., 2002). An approximation of the geoid is the WGS 84 ellipsoid, which is a geocentric equipotential ellipsoid of revolution (NIMA, 1997).

3. GRAVITY FIELD OF THE EARTH

The gravitational field at any point on the earth's surface is composed mainly of gravitation due to the mass of the earth and a centrifugal component due to the rotation of the earth. Furthermore, the gravity fields of the sun and the moon are significant on the surface of the earth.

As the earth is not a perfect sphere, and due to its rotation, the acceleration of gravity is not constant on its surface. Due to that and the variable centrifugal effect, the gravity on the earth's surface varies with

latitude. The non-spherical shape of the earth and local variations of density within the earth (Hunt, 2001) also cause variations. The rotation of the earth and its equatorial bulge produce an increase of gravity with latitude as the centrifugal component of the gravity field is at maximum at the equator and zero at the geographic poles, and the distance from the surface to the centre of mass decreases.

Atmospheric pressure changes also contribute to earth's temporal gravity variation directly by a gravitational effect and indirectly by a deformation effect. Groundwater level, rainfall amount and soil moisture content changes through time add directly to gravitational variations and for large loads, indirect deformation effects are involved (Torge, 1989).

4. GRAVITY SURVEYING AND CORRECTIONS

4.1 Gravity surveying

Regional reconnaissance surveys can have measurements at points several kilometres apart, preferably with uniform distribution, but usually measurement points are along roads. Regional surveys can provide information about major rock unit distribution and deep crustal features of the area covered. To increase the resolution, detailed surveys with denser station distribution are carried out. For survey areas with rapidly changing gravity fields, a denser station spacing is needed, as accurate measurement of gravity gradients is often critical in the subsequent interpretation (Kearey et al., 2002). The necessary interval between stations is dependent on the assumed depth and size of geological features that are expected to create gravity anomalies such as dykes or intrusions, geological contacts, discontinuities and faults.

Accurate measurements of elevation are necessary for corrections of the measurements. An accuracy of station elevation of ±1 cm is needed to achieve accuracies of a few μGals in the gravity values. This precision can be achieved by optical levelling surveys and by the use of differential global positioning system (GPS) surveys (Seigel, 1995). Uncertainty in the elevations of gravity stations probably accounts for the greatest errors in the corrected gravity values on land. Accuracy of the horizontal position of gravity stations on the other hand is far less critical so the latitude of the station should be known to ±10 m (Kearey et al., 2002). In addition, it is important to note that the same reading procedure must be used at every survey point, during each survey. Measurements should preferably not be made during rainy or windy days.

The standard procedure for conducting gravity surveys follows the loop technique. In this technique, a daily field survey starts by measuring at a base or reference gravity station with a known absolute gravity value and ends by measuring at the same base station. In between these measurements, new or previously occupied gravity stations are visited. After the survey is finished, all observed gravity readings are subjected to a reduction or correction process.

Difference in elevations leads to variations in gravity because the gravitational force of the Earth varies with the square of the distance of the survey-point from the centre of the Earth. The higher the elevation h, the smaller gravitational acceleration would be measured (Telford et al., 1990). It is also important to note that the differences in elevation are caused by topographic changes on the earth's surface. Topography also leads to changes in the gravitational acceleration. If a mountain is near the measuring point, it has an upward component of gravity. If a valley is present, a mass is lacking, assuming a correction for a Bouguer plane has been made. This is similar for correction for the sea or bathymetry. Consequently, topographic corrections are always positive or increase in gravity (Lichoro, 2014). A schematic diagram depicting these situations is shown in Figure 1.

Local density variations within the earth affect the gravity as well and cause the anomalies that are the purpose of the surveys. The effect depends on the nature and depth of the material or entity causing these lateral density contrasts. In order to know and explain these variations physically, other factors of

known origin which contribute to changes in the gravitational field should be removed. After they are removed, the anomalies may be interpreted. An example of a gravity anomaly for a hypothetical dense body beneath the surface is shown in Figure 2.

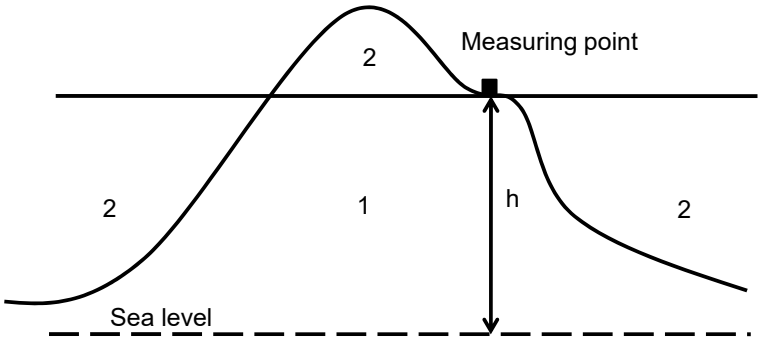

FIGURE 1: The gravity observed at the measuring point (square) of height *h* above the sea level is affected by presence of the hill nearby and valleys on both sides (2) and by the mass underneath it (1)

4.2 Gravity reduction

Gravity reduction is a process used to correct for variations in time and space of the earth's gravitational acceleration, that are not caused by local density differences in the rocks underneath the Earth's surface. The result is reduced gravity readings whose values are on a datum surface such as the geoid or sea-level surface. The corrections are to be made after the observed readings are calibrated based on the calibration factor of the gravimeter used.

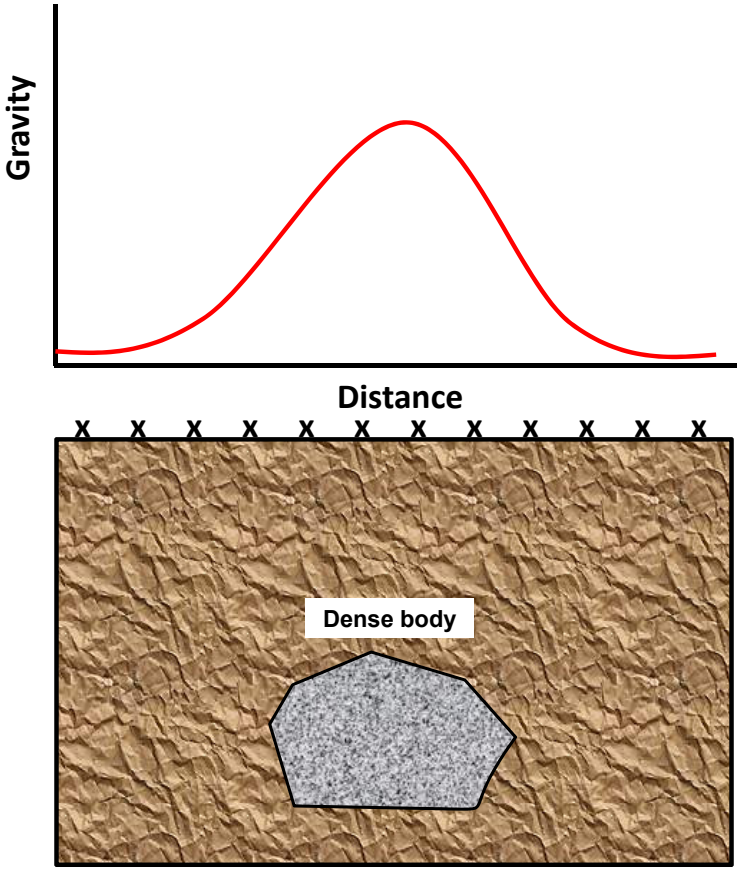

FIGURE 2: Gravity anomaly caused by a buried dense body (modified from Mariita, 2007)

Instrumental drift refers to a change in measured value with time, observable when the gravimeter is left in a fixed location or a measurement is repeated. This phenomenon is due to the imperfect elasticity of the springs inside the gravimeter that undergo creep with time. This can also be caused by temperature variations that, unless counteracted in some way, cause expansion or contraction of the spring and thus give rise to changes in measurements which are unrelated to variations in gravity (Kearey et al., 2002). In order to compensate for the gravimeter drift, repeated measurements at a certain base station are done throughout the day. A drift curve in Figure 3 shows the meter reading at one station against recording time. The drift is assumed to be linear between consecutive base station measurements.

Tidal forces are the direct gravitational forces of the sun and the moon and contribute to the observed gravity field variations of values in the range of about 0.3 mGal and a minimum period of about 12 hours. Tidal correction is made before the instrumental drift is estimated.

As previously mentioned, the non-spherical nature of the Earth's shape contributes to the latitude variation of its gravitational field. Also, as it rotates, a centrifugal acceleration is produced which causes

the gravity to decrease from its poles to the equator. Therefore, any point near the equator is farther from the centre of mass of the Earth and experiences lesser gravitational pull than if it were near the poles. The difference of the gravitational attraction is by some 5.19 mGal. The latitude correction is to be subtracted from the observed gravity readings.

Another correction needed to be accounted for is related to any measurement taken at a certain elevation. As the gravitational acceleration is inversely proportional with the square of the distance, the observed gravity value at a certain height needs to be corrected to a datum sea-level surface. This is resolved by a free-air correction using the formula:

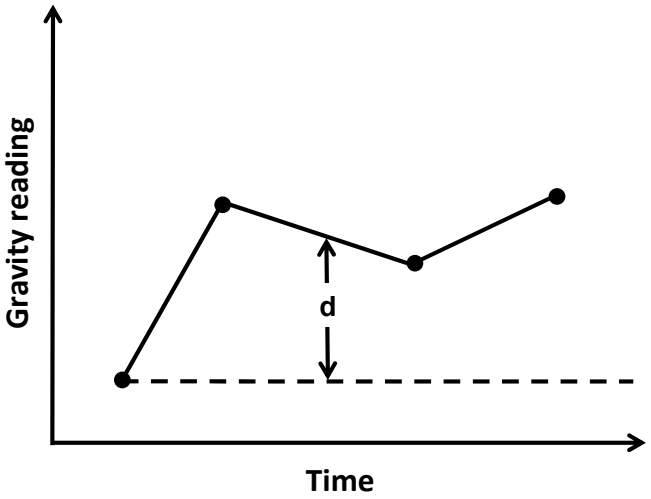

FIGURE 3: Gravimeter drift behaviour (adapted from Kearey et al., 2002)

$$g_{FC} = 0.3086\, h\, mGal \qquad (5)$$

where h = Height of the station measured relative to sea-level [m].

The calculated g_{FC} is then usually added to the observed gravity reading since most of the measurements are above the reference sea-level surface.

Bouguer correction accounts for the mass between the gravity station and the reference level. An infinite horizontal slab is assumed to represent the rock layer beneath the observation point and its thickness is equal to the elevation difference between the observation point and the reference level. The value calculated (Equation 6) will be subtracted from the observed gravity reading at elevation h.

$$g_{BC} = 2\pi G\rho h = 0.04191\, \rho h\, mGal \qquad (6)$$

where ρ = Density of infinite horizontal slab [kg/m^3].

Accounting for effects of topography is important and critical in the gravity reduction process. Hills or mountains reaching above the gravity station exert an upward force on the gravimeter. Valleys are a mass deficit and therefore the Bouguer correction is greater than it should be. In both cases, a correction for these effects is called terrain correction and it is a positive number. One method to account for this correction is the Hammer chart. This is a circular graticule which consists of radial and concentric lines defining several sectors, where the outermost zone extends to 22 km or even farther, beyond which the terrain effects are usually negligible. This transparent graticule is laid out over a topographic map with its centre on the gravity station being observed and the average terrain elevation of each sector is determined. Gravitational effect of each sector is determined and the summation of the gravitational contribution of all sectors contribute to the terrain correction value to be added to the value of the observed gravity (Kearey et al., 2002).

Today, digital maps have been made for many areas. Terrain corrections based on these maps are made by a computer. It is also important to emphasize that in areas of rugged topography, terrain effects are large, being at a maximum in steep-sided valleys, at the base or top of cliffs and at the summits of mountains. This can contribute significant errors as it may be difficult to account correctly for the topographic effect (Kearey et al., 2002). It is therefore advisable to avoid gravity measurements in these areas, if possible.

Atmospheric gravity correction is necessary if the datum level used for reference is the WGS 84 ellipsoid

since this reference ellipsoid encloses the whole mass of the Earth, including atmosphere. With this, the theoretical or normal gravity can be computed at the ellipsoid surface and in space without having to consider atmospheric density differences (NIMA, 1997). The equation for this correction is shown in Equation 7, and it is to be added to the observed gravity reading value:

$$g_A = 0.87e^{-0.116\,h^{1.047}} \tag{7}$$

where h = Elevation with respect to sea level (m).

To summarize, the free-air (g_F) and Bouguer (g_B) gravity anomalies are given by the following:

$$g_F = g_C - g_L + g_A + g_{FC} \tag{8}$$

$$g_B = g_F + g_{TC} - g_{BC} \tag{9}$$

where g_C = Tide and drift corrected gravity values (mGal);
g_L = Normal gravity value with latitude correction (mGal);
g_A = Atmospheric air correction (mGal);
g_{FC} = Free-air correction (mGal);
g_{TC} = Terrain correction (mGal);
g_{BC} = Bouguer correction (mGal).

5. APPLICATIONS OF GRAVITY SURVEYS TO GEOTHERMAL PROSPECTING

Gravity surveys shed light on the structure and physical properties of geothermal fields. The gravity anomalies observed may be due to subsurface geologic features such as lithological contacts, boundaries, faults, dikes, intrusions, and calderas. They can also be due to a change in the physical conditions such as the existence of steam cap (Nordquist et al., 2010). Furthermore, change in gravity because of extraction of fluid can be observed (Eysteinsson, 2000).

Subsurface faults that have no evidence on the surface were delineated and other faults were confirmed in a gravity survey using horizontal gradient analysis of the gravity data collected in the Ungaran Volcano geothermal field in Indonesia (Setyawan et al., 2015). Regional faults were delineated in Hohi geothermal area, Japan, using horizontal gradient interpretation of gravity data (Salem et al., 2005). First and second horizontal gradient methods applied to gravity data from Cipinas geothermal prospect, Indonesia (Martakusumah et al., 2015) also revealed lateral boundaries of density contrasts that may be related to relatively deep faults or geological boundaries within the subsurface.

Dense intrusions and dikes in the Hengill geothermal field have been inferred by correlating gravity anomaly maps with MT resistivity maps. These geological features, perceived to be deep conductors, are reflected as regions with high gravity values (Hersir et al., 2009). Analysis of gravity maps and magnetic maps have also revealed dike intrusions which may serve as heat sources, such as in the Olkaria geothermal field, Kenya (Mariita, 2011).

Geothermal reservoirs of existing geothermal fields are also being monitored by conducting microgravity surveys. These surveys aim to quantify temporal gravity changes associated with continuous exploitation. These temporal variations of gravity values may be caused by mass changes in the geothermal reservoir, vertical ground movements such as subsidence or inflation and groundwater level variations (Hunt, 2001). Mass changes due to liquid drawdown and saturation level changes in the two-phase zone were reported to be the possible reason for the decreased gravity values measured at Tongonan geothermal field, Philippines (Apuada and Olivar, 2005). Subsurface fluid dynamics such as in geothermal reservoirs were also studied in Semarang alluvial plain in Indonesia (Sarkowi et al., 2005) and in Ogiri geothermal power plant, Japan (Nishijima et al., 2015) by time-lapse four-dimensional and hybrid microgravity measurements. Refinement of a geothermal reservoir model was also accomplished by calibrating it against repeated microgravity data (Pearson et al., 2015).

6. MICROGRAVITY SURVEY IN BACMAN GEOTHERMAL FIELD

A microgravity survey was conducted in 2009 and 2010 around the Bacman geothermal field, Philippines. This survey covered a network of 101 gravity stations (Figure 4), using the looping method. Using this method, the daily survey began and ended by doing measurements at the base station. In between, measurements were carried on other gravity stations. Some stations were measured more than once on a trip and in some cases on different trips (Figure 5). At each station, at least three readings were done with difference in dial not exceeding ± 0.3. In this survey, station 77 was used as a base station. The gravity value at station 77 was derived from station 71 where the absolute gravity value is known. Precise levelling survey was conducted in tandem with the gravity survey to determine the elevations of all gravity stations. Appendix I shows location of gravity stations, gravity values and anomalies.

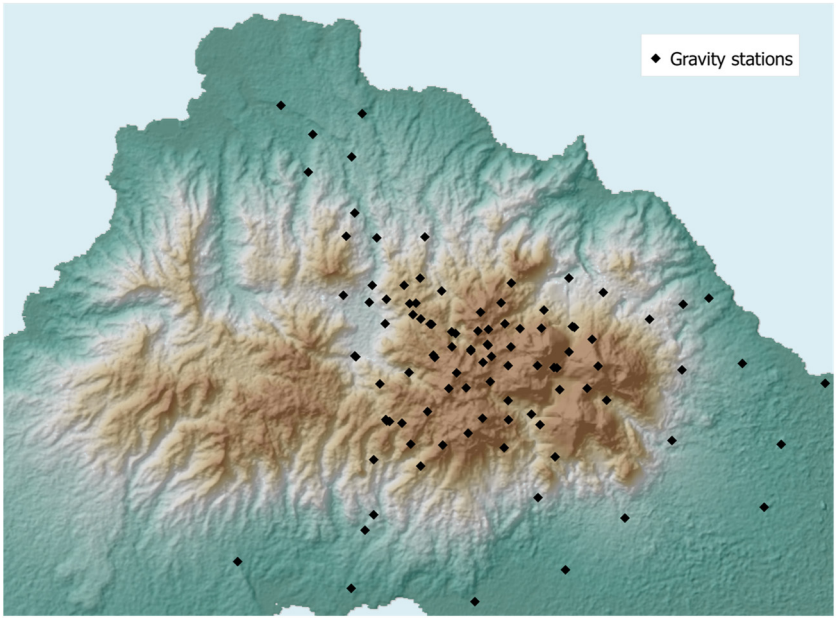

FIGURE 4: Microgravity survey conducted in 2009 and 2010 covering 101 gravity stations in and around the Bacman geothermal field

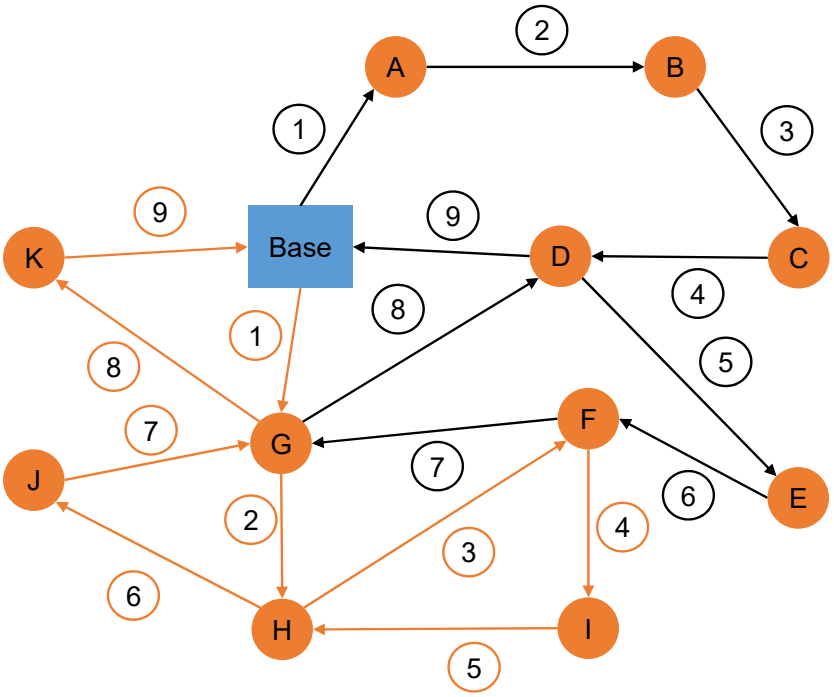

FIGURE 5: A network of gravity stations (orange circles) for two different one-day survey trips; these trips always started and ended at the base station (blue square)

6.1 Microgravity survey data processing

6.1.1 Drift reduction using Gravos reduction program

The Gravos reduction program by Iceland GeoSurvey (ISOR) converts the observed gravity readings of the gravimeter to gravity values. This program calculates the tide correction using the Longman Formula (Longman, 1959). To compensate for the drift of the gravimeter, the drift correction is then calculated for each survey trip. Input parameter files included the summary of the observed gravity readings at each station of each survey trip, the instrument calibration table, the base station with known absolute gravity value, and the gravity stations' coordinates and their corresponding elevations. The output of this will be used for the Gnet reduction program which adjusts the gravity values in a network of gravity stations.

6.1.2 Gravity network adjustment using Gnet program

The Gnet program by ISOR is used to calculate new gravity values of tied or redundant stations measured at least twice by different survey trips. Due to the redundancy of some observations, the gravity measurements need to be adjusted since they may contain gross, random, and systematic errors. These systematic errors are a result of instrument drift, and instrument reading unmodelled calibration factors. In addition, gross errors considered as outliers may be hidden in the data and failure in detecting them may result in false gravity values (Hwang et al., 2002). The Gnet program also calculates the gravity values of all other stations in order to compensate for the newly computed gravity values of tied stations. The program does the calculation by either setting a station with a fixed value as a constraint, or by using no fixed value. The output file of the Gravos reduction program, which corresponds to individual loop drift corrections, will be an input file for the Gnet program. Other input files include the calibration scale factor of the gravimeter used, the observed station readings for the entire survey, the observed station coordinates and elevation. The results of this network adjustment will then be subjected to terrain and elevation corrections.

6.1.3 Latitude, atmospheric air, free-air and Bouguer corrections using Gravity and Bouguer programs

Latitude and atmospheric air corrections are calculated using the Gravity program by ISOR while the free-air and Bouguer corrections were computed via the Bouguer program. The values for these corrections are to be subtracted and added to the observed gravity value, respectively.

6.1.4 Terrain corrections using Terra and Terrb reduction programs

The Terra and Terrb reduction programs by ISOR are used to calculate terrain and bathymetric corrections, respectively. These corrections consider the effect of masses related to land and sea topographic reliefs within the field and several kilometres away from it. However, the program has a limitation in calculating the terrain correction for each gravity station. The program computes the correction by using the Hammer method which divides the area into several zones, but skips the first two zones near and around the observed station, as it assumes the area is relatively flat within 20 m or there is no topographic relief within that distance. The terrain correction is to be added to the observed gravity value. The output of this program will be used to calculate the free-air and Bouguer corrections.

6.1.5 Reduction density estimation

The Parasnis method (Parasnis, 1952) is used to estimate the reduction density ρ. Generally, this method assumes that the free-air correction is only affected by elevation changes, thus, it will increase linearly with elevation. In addition, the Bouguer anomaly is considered to be a random error of mean value zero. Therefore, the plot of free-air anomaly values against the difference between the product of a constant and elevation values and terrain correction per unit density T for all gravity stations, should follow a straight line (Telford et al., 1990).

7. BACMAN GEOTHERMAL FIELD

7.1 Geologic and tectonic setting

Bacman geothermal field, hereafter referred to as BGF, straddles the boundary between the provinces of Albay and Sorsogon, Region V, Philippines (Figure 6). The geothermal field is within two municipalities; Manito town in Albay and Bacon District in Sorsogon. To the northwest is the Mayon Volcano and to the southeast is Mt. Bulusan. The geothermal field is located within a series of Pliocene to recent andesitic and basaltic volcanoes collectively known as Pocdol Mountains and Pocdol volcanic complex.

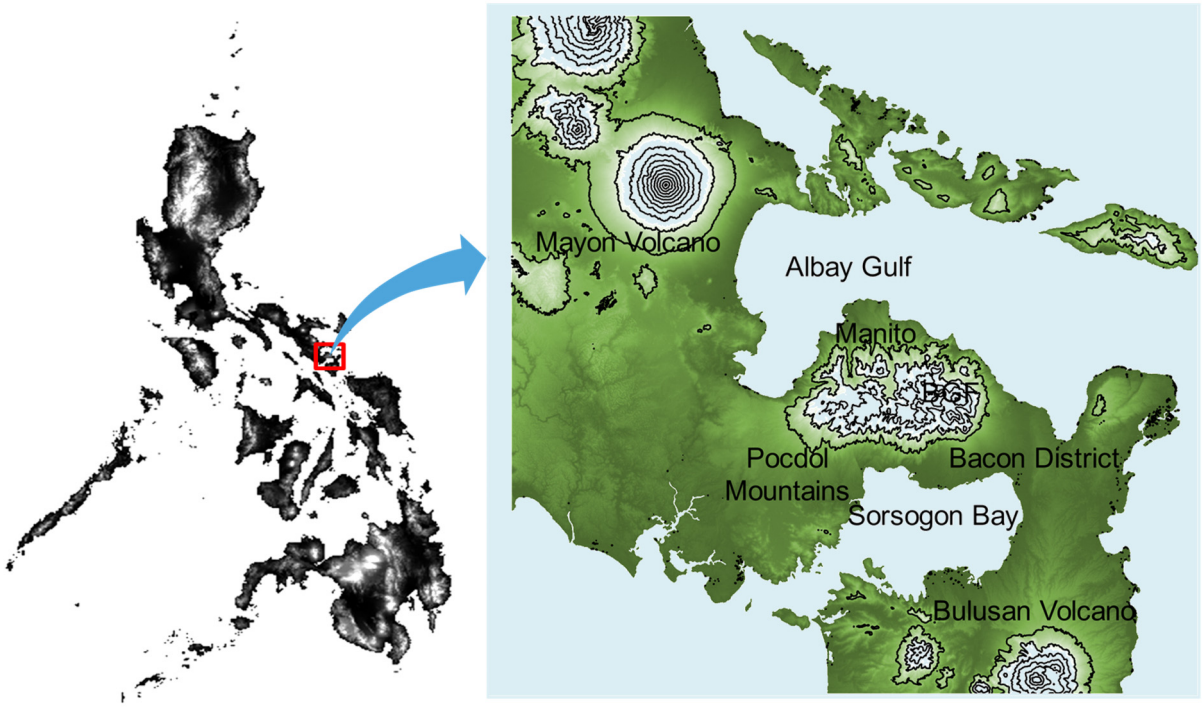

FIGURE 6: Geographical location of Bacman geothermal field, Philippines

The Pocdol volcanic complex is a part of NW-SE trending volcanic chain termed "Bicol Volcanic Belt" which includes Mt. Labo, Mt. Isarog, Mt. Iriga, Mt. Mayon and Mt. Bulusan, as seen in Figure 7. Bicol Volcanic Belt is located between two active tectonic regions. To the east is the Philippine Trench, a subduction zone resulting from the ongoing convergence of the Philippine Sea Plate and the Eurasian Plate, and to the west is the prominent Philippine Fault which runs through the country in a NW-SE orientation. Bacman Fault Zone (BFZ), oriented east-southeast, is a major splay fault of the Philippine Fault, but both faults are active (Lagmay et al., 2005) which affects the geodynamics in the BGF (Figure 8). In the BGF there is extensive faulting, forming graben structures. The geology of the BGF is characterized by volcanic domes and cones, heavily dissected by faults whose attributes and distribution are mainly controlled by the BFZ. In addition, the BGF also contains prominent, eroded collapse features and scarps due to landslides in the western part. The geothermal activities of the BGF appear to be constrained within the BFZ (Braganza, 2014).

Three major lithological formations comprise the BGF. These are: Pocdol volcanics formation (PVF), Gayong sedimentary formation (GSF), and Cawayan intrusive complex (CIC):

- PVF is a sequence of volcanic units composed of lava flows and pyroclastic deposits from numerous volcanic centres of Pliocene to Recent age. PVF is also characterized as slightly to intensely altered andesite lavas and tuff breccias with minor pyroxene basalt.

FIGURE 7: NW-SE alignment of volcanoes locally known as "Bicol Volcanic Belt" (modified from Google Earth, 2015)

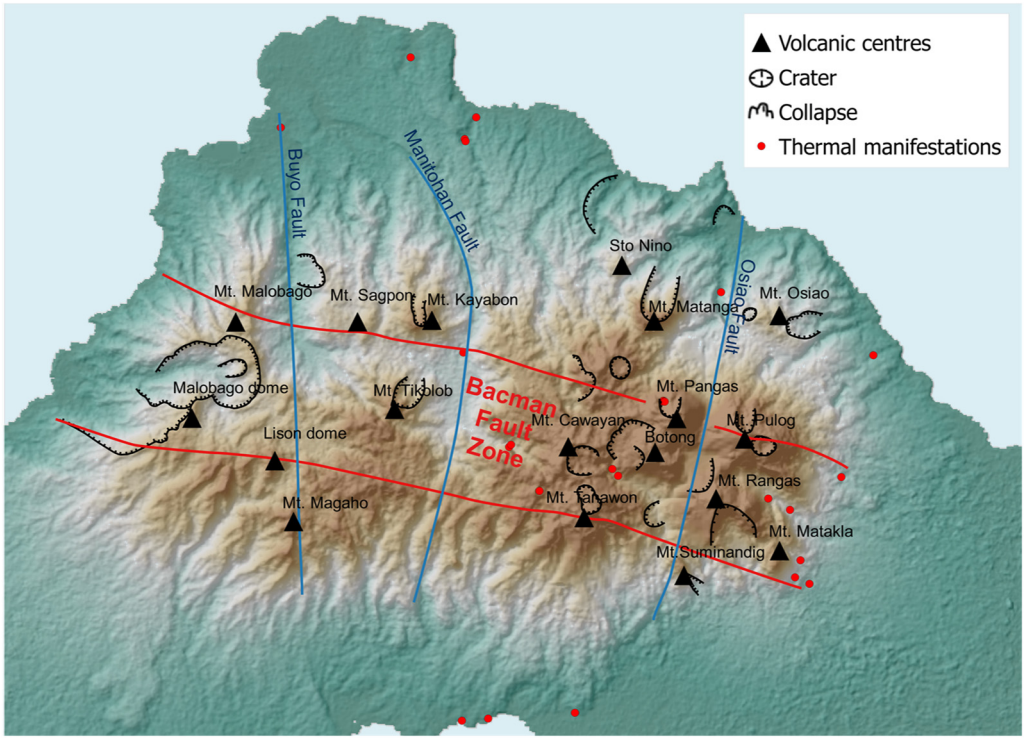

FIGURE 8: Bacman geothermal field elevation map with major tectonic structures, volcanic centres, collapses, craters, and thermal manifestations (modified from Braganza, 2014)

- Beneath the PVF is GSF which is generally described as multi-lithologic units composed of calcareous and fossiliferous sedimentary breccias with volcanic clasts, and dark fossiliferous uniformly-grained and impervious siltstones.
- CIC on the other hand is composed of porphyritic microdiorite, diabase and pyroxene-andesitic rocks and intrudes both PVF and GSF (Santos and Dimabayao, 2011).

7.2 Previous geophysical surveys

Several geophysical surveys have been conducted in Bacman geothermal field since 1970. Regional Schlumberger resistivity traversing (SRT) surveys were conducted in the 1970s into early 1980s and vertical electrical sounding (VES) surveys were done in 1982-1985. In 1996, regional, microgravity, and precise levelling surveys were conducted within and outside the geothermal field, covering a total of 162 temporary and 80 permanent gravity stations. Results from these surveys (Figure 9) show a large positive gravity anomaly across BGF (Tugawin et al., 2015). Several magnetotelluric (MT) and transient electromagnetic (TEM) surveys were carried out in this field from 1999 to 2012. These surveys were conducted in different areas of the geothermal field. The most recent MT survey was done in 2014 covering 75 stations in the eastern part of the field.

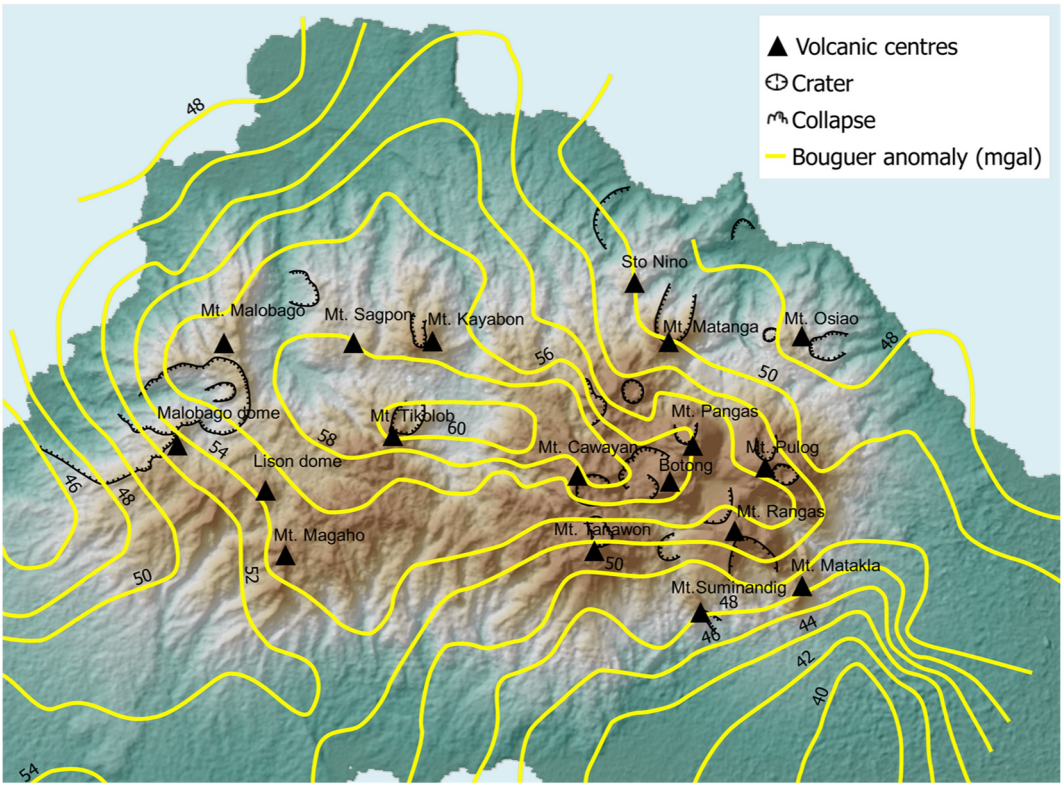

FIGURE 9: Bouguer anomaly map of Bacman geothermal field based on the 1997 regional and microgravity surveys (modified from Tugawin et al., 2015)

8. RESULTS, ANALYSIS AND INTERPRETATION

8.1 Reduction density estimation

A plot (Figure 10) based on Parasnis method shows how the gravity values are distributed. The best fitting line is 2.67 g/cm^3 and this value was computed using the trend1d function of Generic Mapping Tools (GMT) in Linux. The slope is the density that will be optimal in Bouguer and terrain corrections.

Another method of estimating this is by using the Nettleton method (Nettleton, 1939). A SW-NE profile across a prominent topographic feature of the area is generated (Figure 11). Various reduction densities were used to calculate the Bouguer anomalies and are plotted with the topography (Figure 12). By visual inspection, the gravity profile with the least correlation to topography would represent optimal density. The density of 2.67 g/cm^3 is the best choice as in the case of the Parasnis method.

The density of surface rocks can also be measured by collecting samples in the area and measuring the density using laboratory techniques. However, these samples may be eroded due to weathering which can generate a different estimated density values. Also, the density of rocks at depth is different from the rocks at the surface due to variability in water content and compaction (Parasnis, 1986).

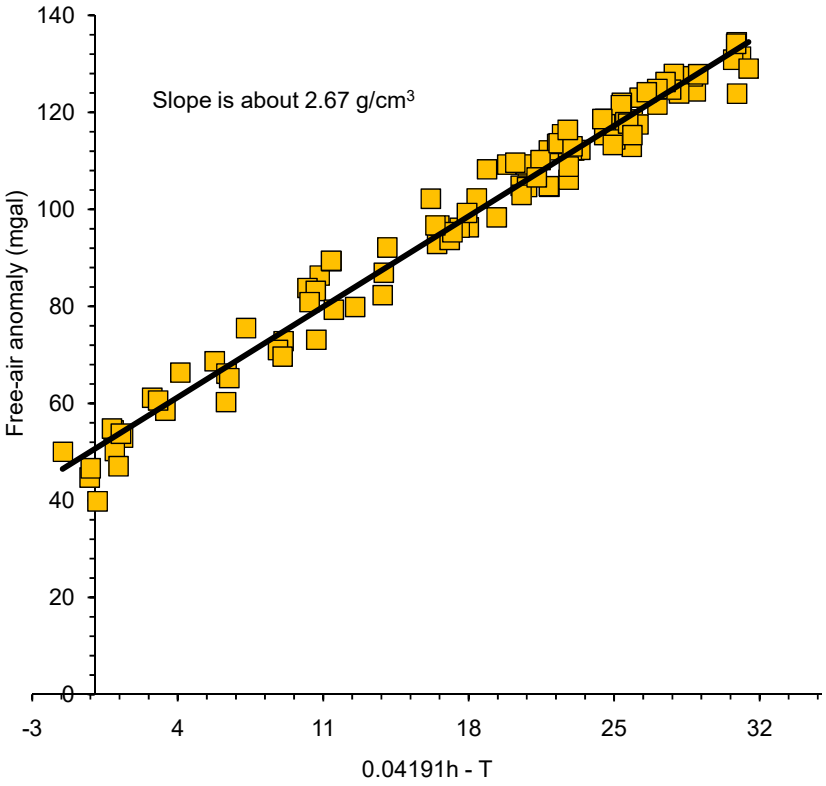

FIGURE 10: Parasnis method to determine the optimum reduction density

8.2 Free-air and Bouguer maps

Free air and Bouguer anomaly maps (Figures 13 and 14) were generated. As seen in Figure 13, relatively high contour values for the free-air anomalies generally correlate with the high topographic reliefs such as the volcanic centres in the middle and relatively low values correspond with low topographic reliefs like plain landforms of the area.

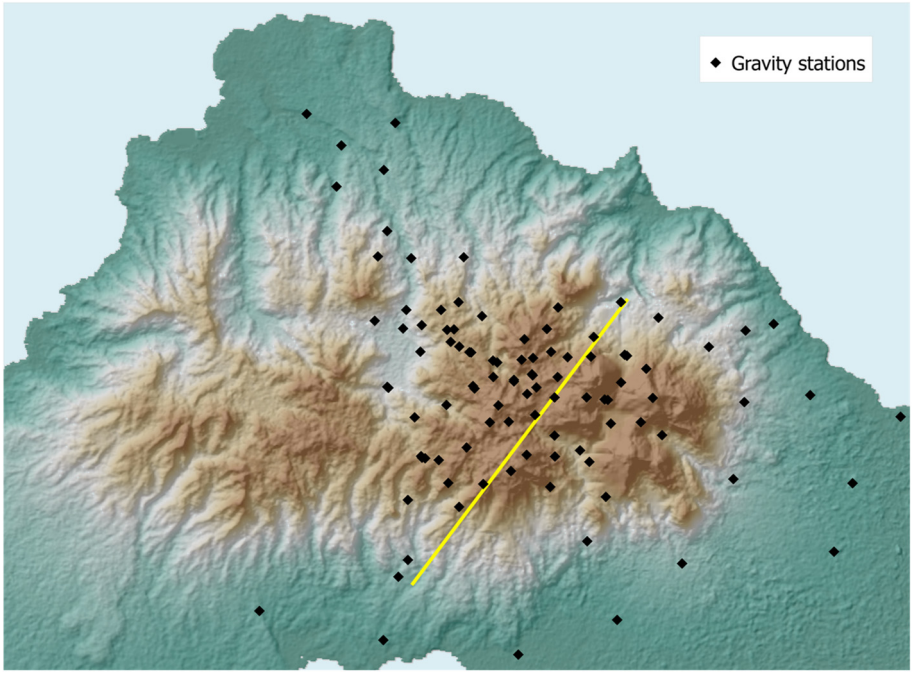

FIGURE 11: Profile (yellow line) used for the Nettleton method

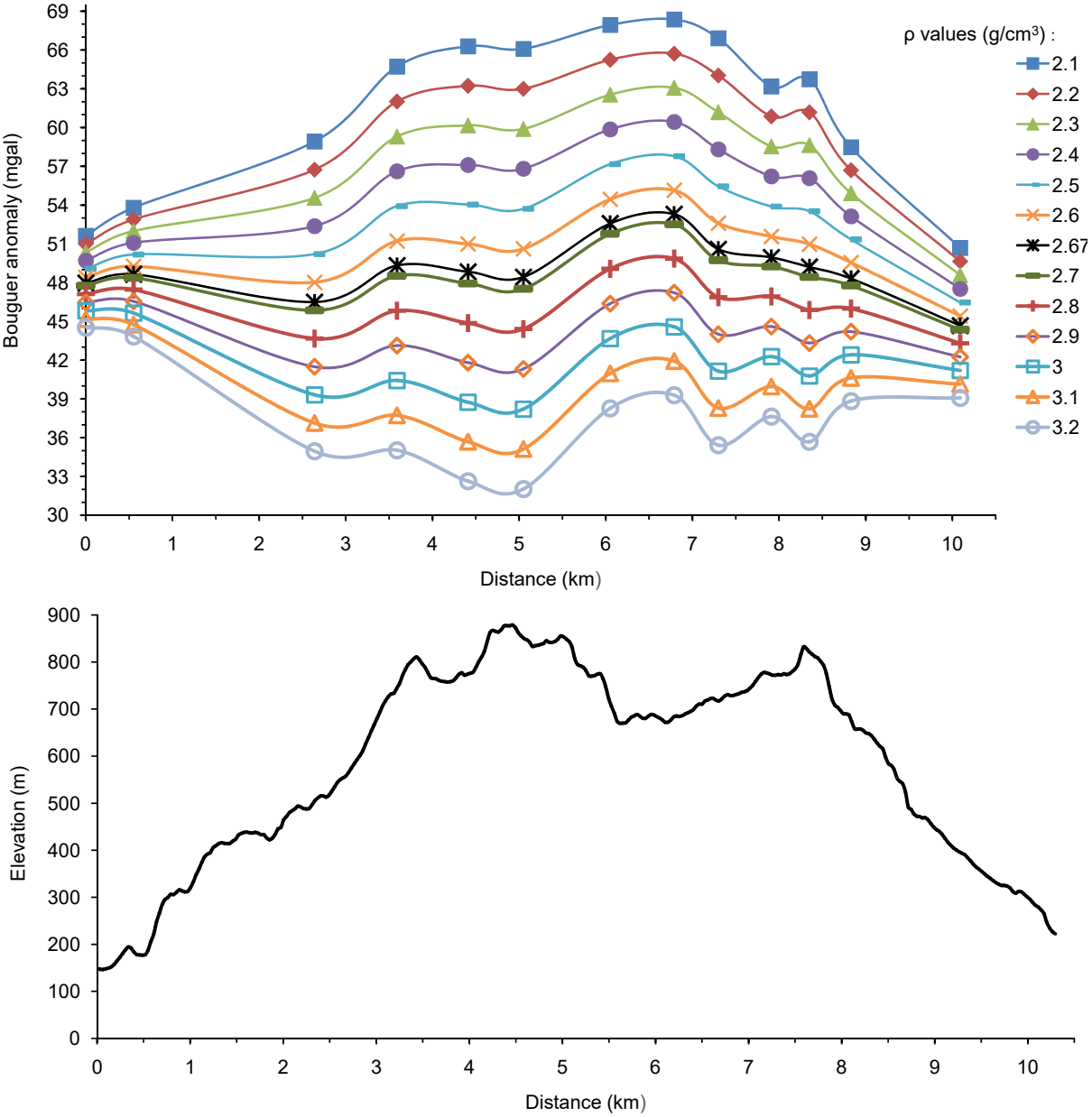

FIGURE 12: Plots of calculated Bouguer anomalies using various reduction densities ρ (top) are compared with the cross-section of the topographic profile (below)

On Figure 14, a relatively high Bouguer anomaly is prominent at the centre of the area near Mts. Cawayan and Botong, and is oriented in the E-W direction. It is also evident that this gravity high is within the BFZ (red lines). The BFZ is actually a main shear zone related to the Philippine Fault and it has many hydrothermal manifestations, caldera structures and volcanic cones (Braganza, 2014). An extension of this broad gravity anomaly extends to the north near Mts. Kayabon and Tikolob. Relatively low gravity values are observed in the southeast region of the area as well as in the northern parts.

8.3 Residual anomaly map

The residual field (Figure 15) is generated by removing the regional field in the Bouguer field. A planar polynomial surface was generated to represent the regional gravity field and the difference between it

and the Bouguer values is the residual field. Higher order polynomials were also tested to model the regional field. It turned out that higher order polynomial planes did not change the residual much. Since there is always a danger of higher order polynomials following the local anomalies, it was decided that planar region field was the most robust and safe. This calculation was done using the Generic Mapping Tool (GMT) grdtrend function in Linux.

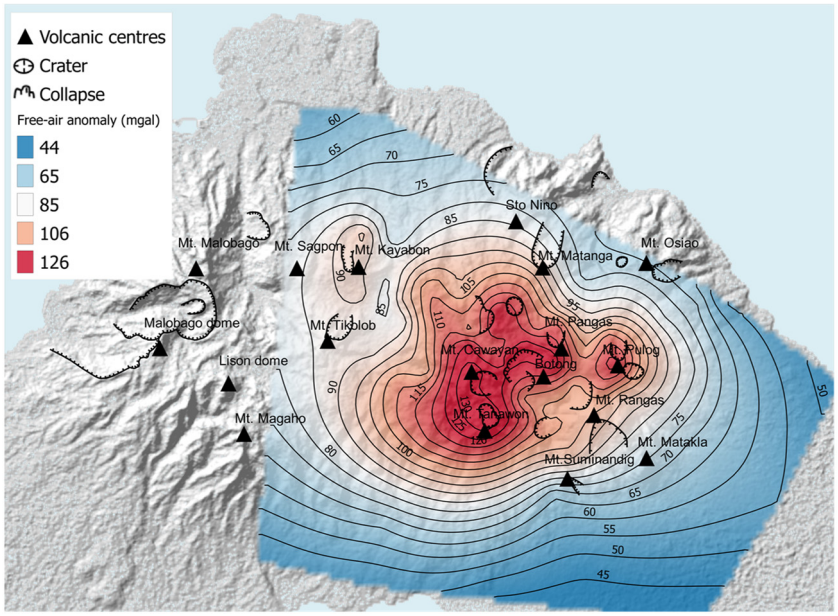

FIGURE 13: Free-air anomaly map of the Bacman geothermal field; the red regions represent high gravity values and the blue regions have low values

Various positive gravity anomalies are observed in the area particularly in the central and western parts. Broad negative gravity anomalies are situated in the northern and south-eastern regions of the field.

The positive anomalies in the central part of the field coincide with the several active hydrothermal manifestations such as solfataras, altered ground, and hot springs. These anomalies are within the BFZ and are near Mts. Botong and Cawayan.

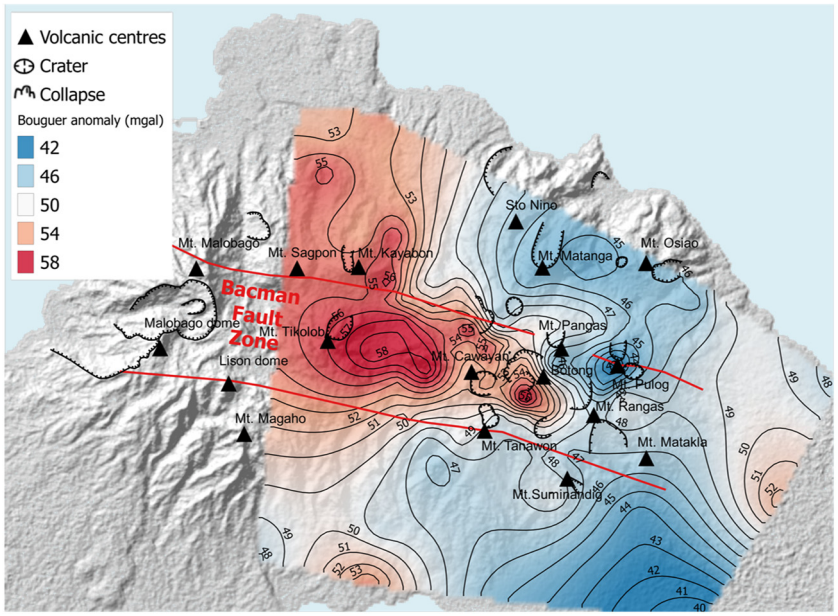

FIGURE 14: Terrain-corrected Bouguer anomaly map of Bacman geothermal field; the red regions correspond high gravity values while the blue regions represent low values

It is also inferred that an upflow zone exists below this area (Ramos and Santos, 2012). Dense intrusive rocks such as diorites are present beneath this area, based on core samples. In addition, positive anomalies also extend to the western and northern parts near Mts. Kayabon and Tikolob and they may be related to the resistivity anomaly seen in the western part of the field (Tugawin et al., 2015). It is also important to note that the high positive anomalies in the central region of the field are separated from the high positive anomalies in the western and northern regions by a narrow zone of lower gravity.

The negative anomalies indicated by blue regions in Figure 15 represent the sedimentary formations and collapse features in the south-eastern and northern parts of the area, respectively. These sedimentary formations are reported to be present particularly in the vicinity of Mt. Rangas (Braganza, 2014).

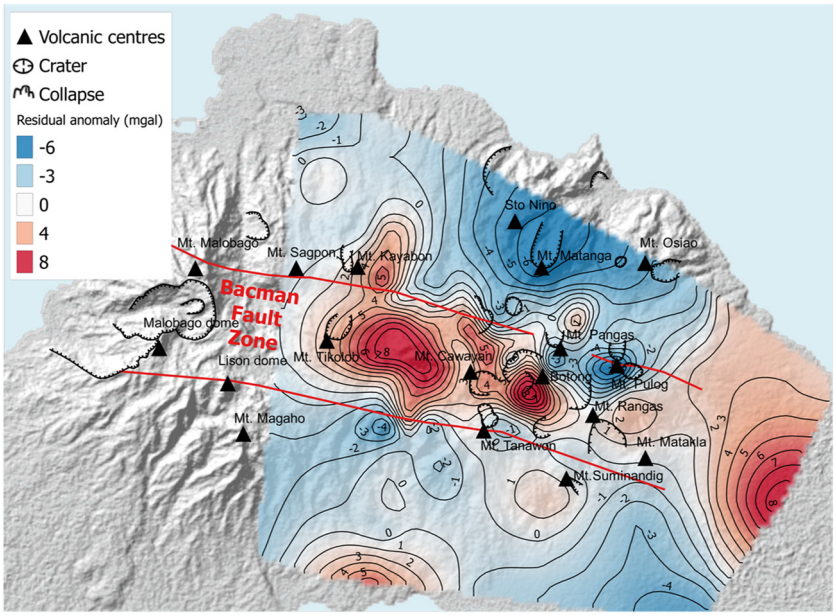

FIGURE 15: Residual anomaly map of the Bacman geothermal field; the red regions correspond to relatively positive numbers while the blue regions represent relatively negative values

9. LIMITING DEPTH ANALYSIS

In order to quantitatively interpret the anomalies, the limiting depth analysis of any dense regular body, can be used, such as the half-width method. This method was applied to the gravity anomaly (Figure 16) at the central part of the field where the dense intrusive rock lies beneath. Assuming this intrusive rock to be a buried regular sphere, the limiting depth z is calculated by:

$$z = 1.302 \times x_{1/2} \tag{10}$$

where $x_{1/2}$ = Horizontal distance from the anomaly maximum to the point at which the anomaly has reduced to half of its maximum value [m].

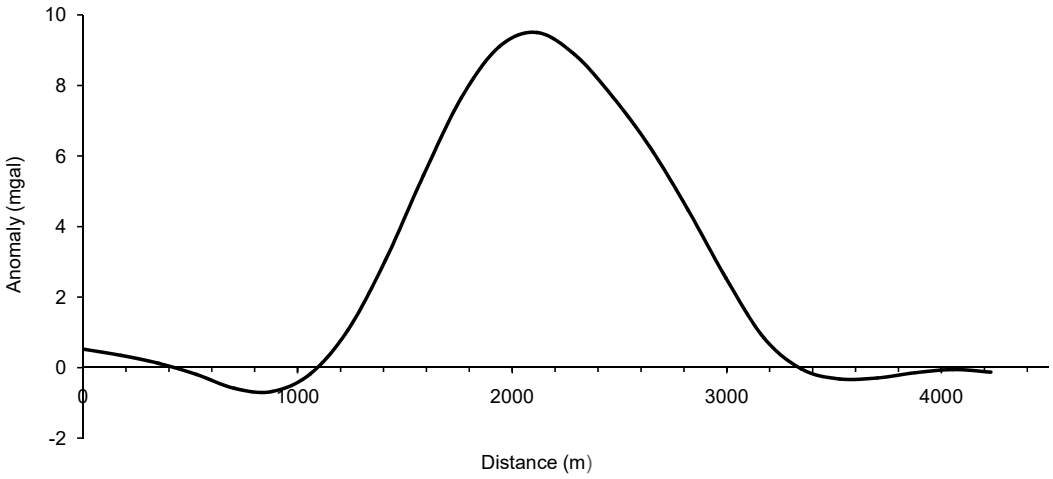

FIGURE 16: Gravity response of a dense body beneath the central part of the Bacman geothermal field

Using Equation 10, the calculated limiting depth is about 900 m. Note that this depth is the distance from the surface to the centre of mass of the buried sphere. Using a simple shape such as a sphere is useful as a first approximation for cases of three-dimensional bodies which are almost symmetrical (Telford et al., 1990).

Meanwhile, for a buried dense body which is assumed to be irregularly shaped, a maximum depth to the top of the body z is computed by the gradient-amplitude ratio method which is:

$$z \leq 0.86 \times \left({}^{A_{max}}/_{A'}\right) \tag{11}$$

where A_{max} = Peak height of the anomaly [mgal];
A' = Maximum slope of anomaly [mgal/m].

This method was applied to an anomaly at the western part of the field wherein an unknown dense body might be present (Figure 17). Assuming it to be irregularly shaped, the maximum depth to the top of this unknown dense body was computed to be about 1750 m.

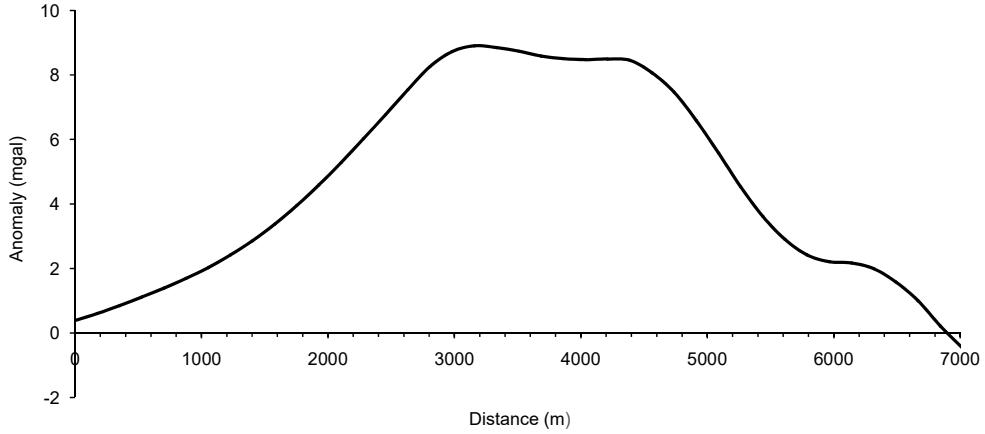

FIGURE 17: Gravity response of a dense body beneath the western part of the Bacman geothermal field

It is important to note that interpretation of gravity anomalies suffers from a non-uniqueness problem, as all geophysical methods. This means that a gravity anomaly can be interpreted by many models. Also, this problem is additional to other uncertainties arising from lack of, or poor quality of data, or interference from other anomalies. Even though the anomaly due to any specified body can be calculated uniquely, one cannot obtain a unique model from an anomaly (Mussett and Khan, 2000). Thus, it is always important to keep in mind that the assumption of the shapes of these dense bodies must be geologically plausible and all available data is needed for a better and accurate modelling. In reality, the shapes of these dense bodies are not simple and symmetrical so more complex modelling tools are required for finer and more precise interpretation.

10. CONCLUSIONS

Microgravity data from the Bacman geothermal field was processed, including tidal and instrumental drift corrections, latitude corrections, atmospheric air, free-air, Bouguer and terrain corrections, and carried out in a Linux environment. Parasnis and Nettleton methods were utilized to estimate the optimum reduction density which was used in the calculations of Bouguer anomalies. Free-air and Bouguer maps were produced. Residual anomaly maps were also generated by removing the regional trend in the terrain-corrected Bouguer maps using a planar polynomial model. Positive anomalies in the central part of the field are within the Bacman Fault Zone. These are interpreted to be dense intrusive rocks such as diorite which are present beneath this area based on core samples. In addition, these anomalies extend to the western and northern regions of the field near Mts. Kayabon and Tikolob. They may be related to the resistivity anomaly found in the western part of the field. Negative anomalies represent the sedimentary formations and collapse features in the south-eastern and northern parts of the area, respectively.

To quantitatively interpret these anomalies, a limiting depth analysis using the half-width and gradient-amplitude ratio methods was done. A sphere model was used for the dense intrusive rock beneath the central region of the field and the computed depth to its centre was around 900 m. Also, the anomaly in the western part of the field was modelled as an irregularly shaped body and the calculated depth to its top was about 1750 m. Note that these methods are very crude in interpretation since they only use simple shapes to represent the anomalies.

ACKNOWLEDGEMENTS

I would like to express my utmost gratitude to the UNU-GTP staff for making this six-month training interesting and more enjoyable. This training was quite a memorable experience for me and my co-fellows. The additions of the project management topic in the Introductory Lectures and group project work in the training were a bit of a surprise for us but we are proud to be the first to have them. A sincere thank you is due to Mr. Lúdvík S. Georgsson, current director of UNU-GTP, for sharing his knowledge, experience, and ideas to us in achieving our objectives in this training. Keep up the good work! It is inevitable to appreciate the dedication and hard work of my supervisors Mr. Kristján Ágústsson and Mr. Ingvar Thór Magnússon. Thank you for your patience in teaching me the basics and complexities of gravity data processing and interpretation. I really learned a lot about gravity corrections using your programs and Linux. You both really pushed me to use Linux and I am thankful for that. Special thanks also to Mr. Gylfi Páll Hersir, the MT method expert, for your patience and guidance to me and my co-geophysicists fellows. You are a good teacher and a great person. Thank you for the home-made ice cream and blueberry cake! It has been a great pleasure as well to work with Mr. Knútur Árnason, the TEM method expert, for sharing his expertise in this method and in Linux as well. To the lecturers from ISOR and other companies of the Introductory Courses and Specialized Trainings, I tip my hat to you all, thanks for the knowledge and experience.

To the UNU-GTP staff Ingimar, Markús, Thorie, and Frída, “takk fyrir” for being patient to us UNU Fellows during our stay in school and fieldtrips. To my co-geophysicist Fellows Ali of Comoros, Amali, and Getenesh, thank you for sharing your ideas and experiences. Of course, most importantly, thanks for your friendship and kindness. I hope we will see each other someday. To the other Fellows, namely Fredrick, Antonio, Hamda, Patrick, Davar, Nyaso, John, Ruth, Anthony, Ali of Djibouti, Fridah, Elizabeth, Aloysius, Pedro, Tingting, Andres, Nuno, Reuben, Fardaneh, Kondwani, Peketsa, Shammah, and Kasu, thank you for the memories and experiences together.

To my colleagues at EDC and co-Fellows, my brothers, Jason, Jigo and Bryan, I am thankful to have experienced this six-month training with you guys. I am proud of you all. To my supervisor Mr. Carlos Emmanuel Los Baños, thank you for giving me this opportunity to go and be trained in Iceland. To Sir Domie also, I know you are in Heaven, thanks for believing in me. To the GREG management namely Mr. Manny Ogena, Mr. Francis Sta. Ana, Mr. Noel Salonga, and Mr. Jeff Caranto, thank you for the support you gave for this training. To my co-EDC employees, thanks are due to all of you for the support and assistance before and during this training: Boyie, Mike, Ado, Randy, Jepoy, David, Gab, Verge, Rocelle, Rod, Suzette, Grace, Bea, Lei, Menchie, and Isay. To all the Filipinos who we met in Iceland, thank you very much for your kindness, for sharing your home with us, and for giving us moral support during this training. I will cherish our good times and bad times together and I will never forget you all.

I am also very thankful to my family, my mother Elena, sister Janine, brothers James and Jay, thank you for your love and care. Most especially, I thank my wife Jenny and daughter Jenny Lee, for the never ending love and support for me in the entirety of this training. You are my motivation and strength to go on. I love you all very much.

Finally and foremost, I would like to dedicate this report to God. Without Him, everything is possible... Glory to God always…

REFERENCES

Apuada, N.A., and Olivar, R.E.R., 2005: Repeat microgravity and leveling surveys at Leyte geothermal production field, North Central Leyte, Philippines. *Proceedings of the World Geothermal Congress 2005, Antalya, Turkey*, 9 pp.

Bertani, R., 2015: Geothermal power generation in the world 2010-2014 update report. *Proceedings of the World Geothermal Congress 2015, Melbourne, Australia*, 19 pp.

Braganza, J.S., 2014: *Volcano-tectonic evolution of the Bacon-Manito geothermal project, Sorsogon, Philippines*. University of Auckland, MSc thesis, 202 pp.

Eysteinsson, H., 2000: Elevation and gravity changes at geothermal fields on the Reykjanes peninsula, SW Iceland. *Proceedings of the World Geothermal Congress 2000, Kyushu-Tohoku, Japan,* 6 pp.

Flóvenz, Ó.G., Hersir, G.P., Saemundsson, K., Ármannsson, H., and Fridriksson, Th., 2012: Geothermal energy exploration techniques. In: Sayigh, A. (ed.), *Comprehensive renewable energy, vol.7.* Elsevier, Oxford, United Kingdom, 51-95.

Google Earth, 2015: *Map of Bicol volcanic belt.* Google Earth.

Hersir, G.P., Árnason, K., and Steingrímsson, B., 2009: Exploration and development of the Hengill geothermal field. *Presented at "Short Course on Surface Exploration for Geothermal Resources", organized by UNU-GTP and LaGeo, Ahuachapan and Santa Tecla, El Salvador*, 12 pp.

Hunt, T.M., 2001: *Five lectures on environmental effects of geothermal utilization.* UNU-GTP, Iceland, report 1-2000, 109 pp.

Hwang, C., Wang, C.G., and Lee, L.H., 2002: Adjustment of relative gravity measurements using weighted and datum-free constraints. *Computers & Geosciences, 28*, 1005–1015.

IEA, 2014: *Key world energy statistics 2014*. OECD Publishing, Paris, France, 80 pp.

Kearey, P., Brooks, M., and Hill, I., 2002: *An introduction to geophysical exploration* (3rd ed.). Blackwell Publishing, Massachusetts, USA, 262 pp.

Lagmay, A.M.F., Tengonciang, A.M.P., and Uy, H.S., 2005: Structural setting of the Bicol basin and kinematic analysis of fractures on Mayon Volcano, Philippines. *J. Volcanology and Geothermal Research, 144,* 1-14.

Lichoro, C.M., 2014: Gravity and magnetic methods. *Presented at "Short Course IX on Exploration for Geothermal Resources", organized by UNU-GTP, GDC and KenGen, Lake Bogoria and Lake Naivasha, Kenya*, 8 pp.

Longman, 1959: Formulas for computing the tidal accelerations due to the moon and the sun. *J. Geophysical Research Atmospheres, 12,* 2351-2355.

Lund, J.W., and Boyd, T.L, 2015: Direct utilization of geothermal energy 2015 worldwide review. *Proceedings of the World Geothermal Congress 2015, Melbourne, Australia*, 31 pp.

Mariita, N.O., 2007: The gravity method. *Presented at "Short Course II on Surface Exploration for Geothermal Resources", organized by UNU-GTP and KenGen, Lake Naivasha, Kenya*, 9 pp.

Mariita, N.O., 2011: Exploration history of Olkaria geothermal field, by use of geophysics. *Presented at "Short Course VI on Exploration for Geothermal Resources", organized by UNU-GTP, GDC and KenGen, Lake Bogoria and Lake Naivasha, Kenya*, 13 pp.

Martakusumah, R., Srigutomo, W., Suryantini, Pratama, A.B., Trimadona, and Haans, A., 2015: Gravity analysis for hidden geothermal system in Cipanas, Tasikmalaya Regency, West Java. *Proceedings of the World Geothermal Congress 2015, Melbourne, Australia*, 9 pp.

Mussett, A.E., and Khan, M.A., 2000: *Looking into the Earth: An introduction to geological geophysics*. Cambridge University Press, UK, 492 pp.

Nettleton, L.L., 1939: Determination of density for the reduction of gravimeter observations. *Geophysics, 4*, 176-183.

NIMA, 1997: *World Geodetic System, 1984, its definition and relationships with local geodetic systems* (3rd ed.). National Imagery and Mapping Agency (NIMA), Department of Defence, Washington DC., US, Techn. Report TR 8350.2.

Nishijima, J., Oka, D., Higuchi, S., Fujimitsu, Y., Takayama, J., and Hiraga, N., 2015: Repeat microgravity measurements using absolute and relative gravimeters for geothermal reservoir monitoring in Ogiri geothermal power plant, South Kyushu, Japan. *Proceedings of the World Geothermal Congress 2015, Melbourne, Australia*, 5 pp.

Nordquist, G.A., Acuña, J., and Stimac, J., 2010: Precision gravity modeling and interpretation at the Salak geothermal field, Indonesia. *Proceedings of the World Geothermal Congress 2010, Bali, Indonesia*, 8 pp.

Parasnis, D.S., 1952: A study of rock density in the English Midlands. *Mon. Not. R. Astron. Soc. Geophysics. Suppl., 6*, 252-27.

Parasnis, D.S., 1986: *Principles of applied geophysics* (4th ed.). Chapman and Hall, NY, US, 402 pp.

Pearson, S.C.P., Franz, P., and Clearwater, J., 2015: Strategy of 4D microgravity survey for the monitoring of fluid dynamics in the subsurface. *Proceedings of the World Geothermal Congress 2015, Melbourne, Australia*, 7 pp.

Ramos, S.G., and Santos, B.N.E.A., 2012: Updated hydrogeological model of the Bacon-Manito geothermal field, Philippines. *Proceedings of the 37th Workshop on Geothermal Reservoir Engineering, Stanford University, Stanford, CA, US,* 4 pp.

Salem, A., Furuya, S., Aboud, E., Elawadi, E., Jotaki, H., and Ushijima, K., 2015: Subsurface structural mapping using gravity data of Hohi geothermal area, Central Kyushu, Japan. *Proceedings of the World Geothermal Congress 2015, Melbourne, Australia*, 6 pp.

Santos, B.N.E.A., and Dimabayao, J.J.T., 2011: Paleoenvironment reconstruction of the Gayong sedimentary formation, BacMan geothermal field, Philippines. *Proceedings of the 33rd New Zealand Geothermal Workshop, Auckland, New Zealand*, 7 pp.

Sarkowi, M., Kadir, W.G.A., and Santoso, D., 2005: Strategy of 4D microgravity survey for the monitoring of fluid dynamics in the subsurface. *Proceedings of the World Geothermal Congress 2005, Antalya, Turkey*, 5 pp.

Seigel, H.O., 1995: *A guide to high precision land gravimeter surveys* (2nd ed.). Scintrex, Ltd., Ontario, Canada, 122 pp.

Setyawan, A., Yudianto, H., Nishijima, J., and Hakim, S., 2015: Horizontal gradient analysis for gravity and magnetic data beneath Gedongsongo geothermal manifestations, Ungaran, Indonesia. *Proceedings of the World Geothermal Congress 2015, Melbourne, Australia*, 6 pp.

Telford, W.M., Geldart, L.P., and Sheriff, R.E., 1990: *Applied geophysics* (2nd ed.). Cambridge University Press, Cambridge, United Kingdom, 770 pp.

Torge, W., 1989: *Gravimetry.* Walter de Gruyter and Co., Berlin, Germany, 465 pp.

Tugawin, R.J., Rigor, D.M., Los Baños, C.E.F., and Layugan, D.B., 2015: Resistivity model based on 2D inversion of magnetotelluric sounding data in Bacon-Manito, Southern Luzon, Philippines. *Proceedings of the World Geothermal Congress 2015, Melbourne, Australia*, 6 pp.

APPENDIX I: Gravity stations: Location, gravity values and anomalies

Gravity station	Latitude	Longitude	Elevation (m)	Calculated gravity value (mgal)	Free-air anomaly (mgal)	Bouguer anomaly (mgal)
1	13.06225	123.923517	611.02	978218.878	111.75	51.21
2	13.05965	123.942067	836.05	978161.943	124.33	47.12
3	13.056361	123.949056	720.89	978191.597	118.59	49.47
4	13.049861	123.95075	850.94	978160.054	127.42	50.59
5	13.047194	123.945167	806.35	978174.139	127.86	50.35
6	13.054367	123.9413	809.91	978170.109	124.64	49.78
7	13.029567	123.91475	600.87	978221.13	112.17	50.54
10	13.062133	123.921717	552.01	978232.944	107.62	51.95
11	13.057817	123.9249	571.56	978231.329	112.21	53.87
12	13.056367	123.927617	584.59	978228.574	113.53	54.13
15	13.054167	123.933783	546.65	978235.887	109.23	56.24
17	13.049183	123.939267	613.13	978221.51	115.55	55.53
18	13.045517	123.942733	700.39	978201.969	123.07	53.09
19	13.0506	123.944017	662.58	978209.44	118.68	53.12
20	13.0548	123.9443	764.34	978183.442	123.9	48.81
21	13.054972	123.953389	639.14	978210.481	112.32	49.95
22	13.060167	123.960278	506.72	978235.562	96.35	48.31
23	13.055528	123.968389	480.04	978240.173	92.91	48.95
25	13.04839	123.96741	637.65	978203.062	104.7	46.27
26	13.04389	123.96393	721.43	978186.853	114.51	45.84
28	13.046967	123.928917	669.39	978210.55	122.03	54.33
30	13.03822	123.93289	895.87	978152.823	134.51	52.02
37	13.0309	123.956567	509.07	978239.641	102.31	53.21
38	13.038117	123.972567	725.78	978183.692	112.92	43.93
40	13.063383	123.91505	444.66	978255.148	96.66	52.4
41	13.056517	123.914667	316.2	978284.23	86.39	57.5
42	13.047233	123.906233	321.05	978285.336	89.36	58.94
44	13.04275	123.921467	456.5	978256.203	102.19	59.03
45	13.039583	123.9131	545.22	978235.834	109.31	53.96
46	13.028533	123.919383	644.53	978210.806	115.35	49.92
48	13.06915	123.96745	308.86	978273.775	73.17	44.68
49	13.067817	123.950933	636.89	978205.545	106.18	45.27
52	13.067317	123.911	290.62	978289.993	83.84	56.51
53	13.080667	123.91235	226.87	978301.872	75.52	56.09
54	13.103517	123.905233	155.79	978317.913	68.73	53.29
55	13.11565	123.908283	78.6	978334.672	61.2	53.79
56	13.11805	123.885	32.72	978342.14	54.42	51.98
58	13.018267	123.911233	463.64	978247.109	96.27	49.38
59	13.016433	123.9247	601.25	978213.156	104.83	46.5
60	13.002783	123.911183	248.66	978289.428	72.89	48.64
61	13.00744	123.95836	219.7	978291.801	66.14	49.2
62	13.0016	123.98326	174.95	978299.55	60.32	43.43
63	13.02335	123.99682	252.74	978287.087	70.99	47.44
64	13.063333	124.007583	73.83	978325.823	52.96	49.31
65	13.099267	123.892783	125.82	978324.655	66.4	55.41
66	12.98975	123.872133	55.31	978325.877	50.21	47.65
67	12.99845	123.90867	180.37	978302.701	65.27	47.96
68	12.98211	123.90466	6.39	978340.529	50.07	54.17
69	12.97825	123.94015	7.59	978334.64	44.71	45.33

Gravity station	Latitude	Longitude	Elevation (m)	Calculated gravity value (mgal)	Free-air anomaly (mgal)	Bouguer anomaly (mgal)
70	12.9871	123.96615	41.52	978326.855	47.04	44
71	12.9711	124.00146	8.54	978329.154	39.8	39.42
72	13.0045	124.02319	33.12	978337.902	54.81	52.58
73	13.02215	124.02814	38.14	978335.993	53.75	50.36
74	13.03926	124.04083	2.13	978340.639	46.61	47.12
75	13.044936	124.017099	100.02	978322.597	58.54	49.44
77	13.02917	123.91499	596.12	978222.677	112.27	50.98
81	13.059033	123.92265	565.72	978231.171	110.2	52.94
82	13.047617	123.9285	666.91	978210.861	121.56	53.92
83	13.056283	123.928067	585.82	978228.357	113.69	54.07
85	13.06929	123.92475	570.64	978224.488	104.63	49.08
86	13.08087	123.92617	370.65	978268.99	86.98	49.86
87	13.06565	123.93095	475.9	978248.26	99.32	51.47
88	13.050317	123.9442	663.61	978209.036	118.61	53.39
89	13.03838	123.93787	743.09	978193.401	127.96	53.56
90	13.02981	123.94254	902.76	978147.317	131.47	48.44
91	13.02563	123.93839	959.24	978129.125	130.86	48.85
92	13.029017	123.915817	598.45	978222.682	113	51.63
93	13.022317	123.9311	839.72	978156.613	121.61	49.33
94	13.055267	123.969	491.47	978237.447	93.72	48.1
95	13.03475	123.949883	543.67	978235.127	108.32	57.93
96	13.048767	123.939267	622.84	978219.33	116.38	55.6
97	13.053667	123.9349	550.55	978235.045	109.61	55.58
98	13.03175	123.92675	745.98	978189.016	124.73	50.68
99	13.0426	123.93515	892.39	978153.693	134.14	51.75
100	13.049933	123.93385	759.56	978187.121	126.3	52.99
101	13.02935	123.949967	701.88	978195.743	117.95	49.8
102	13.0215	123.9487	636.51	978206.451	108.8	47.91
103	13.0401	123.944783	735.26	978192.798	124.87	52.57
104	13.044583	123.949933	723.85	978195.829	124.21	53.3
105	13.022617	123.921867	696.17	978193.73	114.44	47.57
106	13.062267	123.947983	719.8	978191.109	117.54	47.7
107	13.055083	123.959533	748.28	978182.252	117.75	49.2
108	13.0519	123.97405	736.54	978181.278	113.28	46.73
109	13.065067	123.9773	377.38	978261.666	82.36	45.37
110	13.044017	123.963083	733.62	978183.926	115.34	46.27
111	13.03779	123.96469	584.33	978217.39	103	48.18
112	13.044567	123.95835	902.66	978145.529	129.06	45.07
113	13.044367	123.975733	1017.14	978105	123.85	41.34
114	13.03475	123.978133	522.84	978228.515	95.28	49.3
115	13.027933	123.959017	576.64	978223.009	106.64	49.84
116	13.018883	123.9633	526.56	978229.846	98.39	46.73
117	13.047483	123.905933	322.17	978285.092	89.46	59.06
118	13.062533	123.910133	288.84	978289.7	83.19	54.8
119	13.06455	123.9027	369.87	978273.742	92.14	54.56
120	13.087733	123.90605	281.72	978290.648	80.94	53.31
121	13.08115	123.903583	473.91	978246.907	96.74	52.97
122	13.10988	123.8941	85.64	978331.715	60.64	52.5
123	13.0432	123.999783	328.01	978273.017	79.35	48.64
124	13.06165	124.000183	263.35	978284.029	69.69	45.56
125	13.057483	123.990533	353.02	978266.424	79.91	46.47